Monthly Notices of the ROYAL ASTRONOMICAL SOCIETY

MNRAS **471,** 4228–4233 (2017) doi:10.1093/mnras/stx1928
Advance Access publication 2017 July 27

Modelling the GeV emission of HESS J0632+057

Shu-Xu Yi★ and K. S. Cheng★

Department of Physics, The University of Hong Kong, Pokfulam Road, Hong Kong

Accepted 2017 July 25. Received 2017 July 24; in original form 2017 July 4

ABSTRACT

The binary system HESS J0632+057 was recently detected by *Fermi* to possess orbital-modulated GeV emission. In this paper, we study the possibility that the compact companion of HESS J0632+057 is a pulsar. Under such a presumption, we focus on the high-energy emission mechanism of this system, which is as follows. The pulsar companion travels through the circumstellar disc of the main-sequence star twice in each orbit, when some of the matter is gravity captured. The captured matter develops an accretion disc around the pulsar, and from which the soft photons are inverse Compton scattered by the pulsar wind as the GeV emission from the system. With proper choice of parameters, SED and light curve that are in accordance with observations can be produced. We predict that the light curve of GeV emission has two peaks, the larger one is at around 0.4 after the periastron (or 0.1 after the X-ray maximum), while the smaller one is between phases 0 and 0.1, with integrated flux one-fourth of the larger one.

Key words: binaries: close – stars: emission-line, Be – stars: individual (HESS J0632+057) – gamma-rays: stars.

1 INTRODUCTION

HESS J0632+057 was discovered as a TeV gamma-ray source (Aharonian et al. 2007). The follow-up observations found periodic time variations of emission in X-ray and TeV (Aharonian et al. 2007; Acciari et al. 2009; Hinton et al. 2009; Aleksić et al. 2012; Aliu et al. 2014), which revealed the binary nature of this system. This system is considered to be one of the γ-ray binary systems[1] (see Dubus 2015 for a review). The optical companion is a Be star MWC 148 (Aharonian et al. 2007). Casares et al. (2012) detected the radial velocity variations in the photospheric lines of the optical companion and thus determined the period of the binary system $P = 321 \pm 5$ days and the mass function $f(M) = 0.35^{+0.20}_{-0.15}\,\mathrm{M}_\odot$. Aliu et al. (2014) further refined the orbital period to be 315^{+6}_{-4} days. The mass of the optical companion was determined to be $13.2 - 19.0\,\mathrm{M}_\odot$ (Aragona, McSwain & De Becker 2010). Due to the uncertainty of the inclination of the orbit, the possible mass range of the compact companion is determined to be in the range $1.3 - 7.1\,\mathrm{M}_\odot$, which covers two distinct categories: neutron stars (usually believed to have mass $M_\mathrm{c} < 3\,\mathrm{M}_\odot$; Kalogera & Baym 1996) or black holes. We summarize other aspects of the binary in Section 2.

There are two families of mechanisms to explain the high-energy emission of γ-ray binary systems, depending on the nature of the compact companion. When the compact object is a black hole, accretion from the main-sequence star is expected to produce a microquasar jet, which accounts for the high-energy emission (see a review by Bosch-Ramon & Khangulyan 2009, and references therein). On the other hand, if the compact object is a neutron star (a pulsar), one main branch of theories explains the high-energy emissions to originate from the collision shock between the pulsar wind and the stellar wind/circumstellar disc (CD) (Maraschi & Treves 1981; Dubus 2006).

An example of the pulsar wind scenario is the γ-ray binary system PSR B1259-63/LS2883, where the compact companion is known to be a pulsar for its radio pulsations. Theoretical models on this system (Kong et al. 2011, and references therein) proposed that the X-rays are produced by synchrotron radiation from shock-heated electrons, and TeV emission is produced via an inverse Compton (IC) process of the hot electrons (both synchrotron self-Compton and external IC scattering of the thermal photons from the optical companion). However, to explain the GeV emission (HE, 100 MeV to 100 GeV) is more difficult. Many of the efforts try to explain the GeV emission with IC scattering by cold electrons from the pulsar wind (e.g. Khangulyan et al. 2012; Dubus & Cerutti 2013). The main difficulty is the lack of soft photons because the GeV peaks at ∼20 days after periastron, where neither the circumstellar matter nor the soft-photon field from the optical companion is at the densest. Recently, we use a new approach to the GeV emission of the system (cf. Takata et al. 2017; Yi & Cheng 2017). In that framework, the soft photons are from the accretion disc around the pulsar, which

★ E-mail: yishuxu@hku.hk (S-XY); hrspksc@hku.hk (KSC)

[1] The term 'γ-ray binary' in our paper is equivalent to 'γ-ray emitting binary' with a pulsar or a black hole companion in Dubus 2015. However, the author use 'γ-ray binary' to specifically refer the case when the compact companion is a pulsar.

was developed after the CD matter being gravity captured by the pulsar at disc crossing. The time required for the accretion disc to form corresponds to the lag time between the X-ray/TeV maximum and the GeV peak.

HESS 0632+057 seems to share some observational similarities and therefore researchers put efforts in searching for its GeV emission for a long time. With 3.5 years of data from *Fermi* Large Area Telescope (LAT), Caliandro et al. (2013) found no GeV emission and set the upper limit of the GeV flux for this system. A recent search for HESS J0632+057 with up-to-date *Fermi*-LAT data discovered the orbital-modulated HE GeV emission (Li et al. 2017). With the studies on the Balmer and Fe II line profile variations from the CD, Moritani et al. (2015) concluded that the pulsar wind mechanism is the most likely candidate for high-energy emissions in this system. These motivate us to apply the model proposed for B1259-63/LS2883 to HESS J0632+057.

The presupposition of the model is that the compact object in HESS J0632+057 has a mass of a neutron star. In Section 2, we discuss the mass of the compact object based on the present observational constraints. We also discuss other parameters of the binary system which will be used in the next section. In Section 3, we discuss the mass transfer and accretion process. In Section 4, we calculate the time-dependent HE SED and light curve as a prediction of our model for future test by observations. We conclude and discuss our finding in the final section.

2 MODEL PARAMETERS

In our model, the compact companion of the binary system is a pulsar. When the pulsar travels through the CD, some of the materials are gravity captured by it. An accretion disc then develops around the neutron star, and the soft photons from the accretion disc are IC scattered by the relativistic electrons in the pulsar wind. The upscattered photons are the observed HE emission.

2.1 The parameters of the binary and the circumstellar disc

To explore the validity of the proposed scenario, we first examine the parameters of the system within ranges set by previous observations. Those parameters include the masses of the compact companion M_c and optical companion $M_\star$, the configuration of the orbit, the geometry and the density profile of the CD, the spin property of the pulsar and the velocity distribution of the pulsar wind.

We start with ranges of the parameters of the optical companion and the orbital solution of Aragona et al. (2010) and Casares et al. (2012): $K = 22.5 \pm 5.7\,\mathrm{km\,s^{-1}}$, $M_\star = 16.1 \pm 2.9\,\mathrm{M_\odot}$, $e = 0.83 \pm 0.08$ and $P = 321 \pm 5$ days, where K is the amplitude of the radial velocity modulation, and e and P are the eccentricity and period of the orbit, respectively. The resulted mass function is $f(M) = 0.35^{+0.20}_{-0.15}\,\mathrm{M_\odot}$, where

$$f(M) \equiv \frac{PK^3}{2\pi G}(1-e^2)^{3/2} = M_c^3 \sin^3 i_o/(M_\star + M_c)^2. \quad (1)$$

In the above equation, i_o is the inclination of the orbit. Casares et al. (2012) limited i_o to be within 47°–80°.

Suppose that the distribution of K, $M_\star$ and e is Gaussian and the standard derivative is their given uncertainty (with P fixed to 321 d as in Casares et al. 2012), and $\sin i_o$ is uniformly distributed in its range, we can obtain the distribution of M_c. The probability density distribution of M_c is plotted in Fig. 1. We can see from this figure that the probability of the compact companion to have a mass of

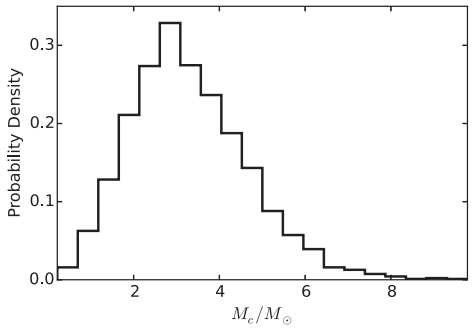

Figure 1. The probability density distribution of M_c based on the observed distribution of K, e, P and $M_\star$.

a neutron star (<3 $\mathrm{M_\odot}$) is less (than that of a black hole) but still significant.

We specify three sets of K, e, P, i_o and $M_\star$ in Table 1. Under each parameter $M_c = 1.5$, 2.0 and 2.4 $\mathrm{M_\odot}$, respectively. The possibilities of $M_c \leq 1.5$, 2.0 and 2.4 $\mathrm{M_\odot}$ are ∼8 per cent, 17 per cent and 28 per cent, respectively.

Next, we discuss the properties of the CD. Outside the CD, we suppose the velocity of the stellar wind is radial and takes the form (Waters et al. 1988)

$$v_w(r) = 10^8\ \mathrm{cms^{-1}} \times (1 - R_\star/r)^{1.5}, \quad (2)$$

and the density profile is

$$\rho_w(r) = \frac{10^{-8}\ \mathrm{M_\odot\ yr^{-1}}}{4\pi r^2 v_w(r)}. \quad (3)$$

The density distribution of the CD has been modelled by previous researchers (Lee, Osaki & Saio 1991; Porter 1999; Carciofi & Bjorkman 2006) as

$$\rho_{CD} = \rho_0 \left(\frac{R_\star}{R}\right)^n \exp\left(\frac{-z^2}{2H^2}\right)$$
$$= \rho_0 \left(\frac{R_\star}{R}\right)^n \exp\left(\frac{-(\phi - \phi_{CD})^2}{2\Delta\phi^2}\right), \quad (4)$$

where n is in the range 3–3.5, with 3.5 corresponding to a steady-state isothermal outflow, H is the scaleheight of the disc and z is the coordinate in the vertical direction of the CD. The second part of above equation is the disc density profile projected to the orbital plane, where ϕ_{CD} is the azimuthal angle at which the mid-plane of the CD intersects with the orbital plane and $\Delta\phi$ is the half-width of the CD projected on the orbital plane. Chernyakova et al. (2006) proposed that $\phi_{cd,\pm}$ and $\Delta\phi$ corresponded to the peak position and the width of the X-ray and TeV light curves. We use $\phi_{cd,+} = 170°$ and $\Delta\phi = 2.2°$ based on the X-ray light curve from Bongiorno et al. (2011). The orientation and inclination of the CD with respect to the orbit plane are important for the determination of the relative velocity between the neutron star and material on CD. Denoting the azimuth angle and the polar angle of the angular momentum vector of CD as φ_n and θ_n, respectively, and the azimuth angle and the polar angle of the direction to the observer as $\varphi_\oplus$ and $\theta_\oplus$, respectively, we have the following equation:

$$\sin\theta_\oplus \sin\theta_n \cos(\varphi_\oplus - \varphi_n) + \cos\theta_\oplus \cos\theta_n = \cos i_{CD}, \quad (5)$$

where i_{CD} is the inclination of the CD with respect to the observer (see Fig. 2 for illustration). There is a relationship between i_{CD} and the full width at zero intensity of certain absorption lines of the inner region of the CD σ_{FWZI}:

$$\sigma_{FWZI}/2 \times |\sin i_{CD}| = (GM_\star/R_\star)^{1/2}. \quad (6)$$

Table 1. Parameters of the model.

	K (km s^{-1})	e	P (d)	i_o (°)	$M_\star$ ($M_\odot$)	M_c ($M_\odot$)	a (km)	$\phi_{cd,+}$ (°)	$\Delta\phi$ (°)
1	16.8	0.88	315	80°	13.2	1.5	3.29×10^8	170°	2.2°
2	19.2	0.86	315	70°	13.2	2.0	3.32×10^8	170°	2.2°
3	22.5	0.88	315	75°	16.1	2.4	3.55×10^8	170°	2.2°

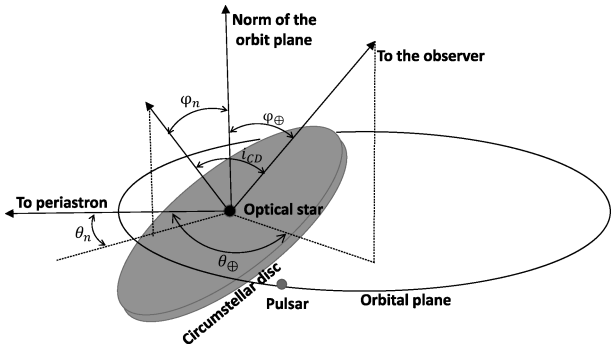

Figure 2. Illustration of the binary system configuration. φ_n and θ_n illustrated in this figure do not represent the values adopted in the text.

Using the measured $\sigma_{FWZI}(\lambda 5018) \sim 1300\,\mathrm{km\,s^{-1}}$ and assuming the radius of MWC 148 to be $R_\star = 6.6\,R_\odot$ (which is in the range of Aragona et al. 2010), we obtain that $i_{CD} = \pm 73°$. Putting $i_{CD} = \pm 73°$ and $\varphi_n = \phi_{CD,+} - 90°$ into equation (5), we have $\theta_n = 75.3°$ and $\varphi_n = 80°$.

2.2 The IC efficiency and the accretion rate of the disc

We define the IC efficiency as the ratio between the luminosity of HE emission that originates from IC and the pulsar wind luminosity:

$$\xi = \frac{L_{IC}}{L_{pw}}. \tag{7}$$

L_{pw} refers to the pulsar wind luminosity in particles, which could be much less than the spin-down power of the pulsar near the pulsar if most spin-down power is still in an electromagnetic wave.[2] ξ is determined by the density of the soft-photon field, which is related with the accretion rate of the accretion disc.

The energy losing rate via IC of an electron through an isotropic photon field is

$$\frac{dE_e}{dt} = -\frac{4}{3}\sigma_T c U_{ph}\Gamma^2, \tag{8}$$

where σ_T is the Thompson scattering section and U_{ph} is the energy density of the photon field. The above equation can be rewritten as the energy losing rate along the light of sight:

$$m_e c^2 \frac{d\Gamma}{dl} = -\frac{4}{3}\sigma_T U_{ph}\Gamma^2. \tag{9}$$

Integrating equation (9), we have

$$\frac{\Gamma_i}{\Gamma_f} = 1 + \frac{4\sigma_T\Gamma_i}{3m_e c^2}\int_0^\infty U_{ph}(l)dl. \tag{10}$$

[2] It is generally believed that the pulsar spin-down power would be converted into the pulsar wind power. However, at the IC location, how much pulsar spin-down power has been converted into the pulsar wind power is not known. As a result, the inferred pulsar wind power is a lower limit of the pulsar spin-down power.

The soft-photon field is constituted by radiation from the accretion disc developed around the pulsar. In the axis of the accretion disc, the integration of U_{ph} along l is

$$\int_0^\infty U_{ph}(l)dl = \frac{4\pi^5 r_{in}}{15c^3h^3}(kT_{in})^4. \tag{11}$$

Substituting equation (11) into equation (10), we have

$$\frac{\Gamma_i}{\Gamma_f} - 1 = 7.43\times10^{-2}\frac{\Gamma_i}{10^3}\left(\frac{kT_{in}}{10\,\mathrm{eV}}\right)^4\frac{r_{in}}{10^8\,\mathrm{cm}} \approx \frac{L_{IC}}{L_{pw}-L_{IC}}. \tag{12}$$

The last approximation relationship in the above equation is due to the fact that the energy of electrons is transferred to the photons via the IC process, with an isotropic assumption. If the accretion disc is a Shakura–Sunyaev disc (Shakura & Sunyaev 1973), then take the relationship between r_{in} and T_{in}:

$$T = 1.4\times10^4\alpha^{-\frac{1}{5}}\left(\frac{\dot{M}_{acc}}{10^{16}\,\mathrm{gs^{-1}}}\right)^{\frac{3}{10}}\left(\frac{M_c}{M_\odot}\right)^{\frac{1}{4}}\left(\frac{r_{in}}{10^{10}\,\mathrm{cm}}\right)^{-\frac{3}{4}}\mathrm{K}, \tag{13}$$

then we have

$$\frac{L_{IC}}{L_{pw}-L_{IC}} = 15.5\alpha^{-0.8}\frac{\Gamma_i}{10^3}\left(\frac{\dot{M}_{acc}}{10^{16}\,\mathrm{gs^{-1}}}\right)^{1.2}\frac{M_c}{M_\odot}\left(\frac{r_{in}}{10^8\,\mathrm{cm}}\right)^{-2}, \tag{14}$$

where α is the viscosity index in the SS disc.

If we take the Alfvén radius r_A as r_{in},

$$\frac{r_A}{10^8\,\mathrm{cm}} = 5.1\left(\frac{\dot{M}_{acc}}{10^{16}\,\mathrm{gs^{-1}}}\right)^{-2/7}\left(\frac{M_c}{M_\odot}\right)^{-1/7}\mu_{30}^{4/7}, \tag{15}$$

where μ_{30} is the magnetic dipole in units of $10^{30}\,\mathrm{G\,cm^3}$. Therefore, equation (14) becomes

$$\frac{\xi}{1-\xi} = 0.6\alpha^{-0.8}\frac{\Gamma_i}{10^3}\left(\frac{\dot{M}_{acc}}{10^{16}\,\mathrm{gs^{-1}}}\right)^{1.77}\left(\frac{M_c}{M_\odot}\right)^{1.29}\mu_{30}^{-8/7}. \tag{16}$$

The above equation relates the IC efficiency with $\dot{M}_{acc}$. With a typical assumption that the IC efficiency is 10 per cent, $M_c = 1.5\,M_\odot$, $\mu_{30} = 1$, $\Gamma_i = 10^3$, $\alpha = 0.1$ and $\dot{M}_{acc} \approx 3.5\times10^{15}\,\mathrm{g\,s^{-1}}$. Note that $\dot{M}_{acc}$ is calculated under the isotropic soft-photon field assumption. When the anisotropic soft-photon field is considered (anisotropic IC, AIC), the needed $\dot{M}_{acc}$ will be higher. The estimation here will serve as an insight into the spectrum calculation in Section 4.

3 MASS TRANSFER AND ACCRETION RATE

The circumstellar material (CM) transfers to the compact star via the Bondi–Hoyle process (Bondi & Hoyle 1944). The transfer rate is

$$\dot{M}_{transf} = \eta\pi r_{BH}^2\rho v_{rel}, \tag{17}$$

where η accounts for the inefficiency of the Bondi–Hoyle accretion, v_{rel} is the relative velocity between the neutron star and the circumstellar material, ρ is the density of CM and

$$r_{BH} = \frac{2GM_c}{v_{rel}^2} \tag{18}$$

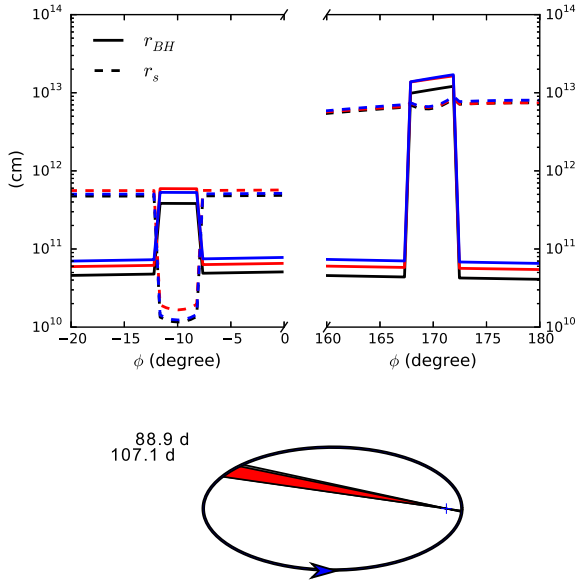

Figure 3. Upper panel: r_s (dashed) and r_{BH} (solid) as a function of ϕ for three sets of parameters, where ϕ is the true anomaly. Black lines are for parameter set 1, red lines are for set 2 and blue lines are for set 3. Bottom panel: The illustration of the orbit and the position of the disc (grey shade region). The red shades are regions where mass transfer takes place. The number beside the orbit is the days after periastron of the start and end of the mass transfer. The sense of orbit is counter clockwise, as indicated with the arrow. Both panels are plotted with $n = 3.5$ and $\rho_0 = 1 \times 10^{-9}$ g cm^{-3}.

is the radius of the Bondi–Hoyle accretion when $v_{\rm rel}$ is much larger than the sound speed of CM. $v_{\rm rel}$ depends on the orientation and inclination of the CD.

However, the collision between the pulsar wind and the stellar wind will alter $v_{\rm rel}$ at a shock-front radius of

$$r_{\rm s} = \sqrt{\frac{L_{\rm pw}}{4\pi\rho v_{\rm rel}^2 c}}. \tag{19}$$

Therefore, a necessary condition for accretion is $r_{\rm BH}/r_{\rm s} > 1$:

$$\dot{M}_{\rm transf} = \begin{cases} 0 & r_{\rm BH} < r_{\rm s} \\ \pi r_{\rm BH}^2 \rho v_{\rm rel} & r_{\rm BH} \geq r_{\rm s} \end{cases} \tag{20}$$

When the neutron star is outside the CD, evaluation from equations (2) and (3) gives $r_{\rm BH}/r_{\rm s} \ll 1$. As a result, mass transfer is impossible outside the CD.

We have assumed in the above section that $\xi = 10$ per cent, and Li et al. (2017) found that the HE luminosity was $\sim 2.7 \times 10^{33}$ erg s^{-1}. As a result, we suppose the pulsar wind luminosity as $L_{\rm pw} = 2.7 \times 10^{34}$ erg s^{-1}. In Fig. 3, we plot $r_{\rm s}$ and $r_{\rm BH}$ as functions of the true anomaly (the upper panel). We also visualize the orbit and the location of the CD in the bottom panel (see details in the caption of the figure).

The transferred materials need to have enough angular momenta for an accretion disc to form. When accrete from the CD, the specific angular momenta of the transferred mass originate from the gradients of the velocity and the density:

$$l = \frac{(GM_{\rm c})^2}{v_{\rm rel}^3}\left(\frac{|\nabla v_{\rm rel}|}{v_{\rm rel}} + \frac{|\nabla \rho_{\rm cd}|}{\rho_{\rm cd}}\right). \tag{21}$$

We evaluate the circular radius with $R_{\rm circ} = l^2/(GM_{\rm c})$ and equation (21), and find that $R_{\rm circ}$ is orders of magnitudes larger than the typical light cylinder radius. Therefore, the angular momenta are enough.

If the duration of mass transfer is much larger than the viscosity time-scale, we expect a stable accretion disc establishing with the accretion rate equal to the mass transfer rate. On the other hand, if the duration of accreting is much less than the viscosity time-scale, we expect the accretion disc is transient and the accretion rate at the inner edge of the accretion disc is described as follows (Rees 1988):

$$\dot{M}_{{\rm acc},\delta} \propto \begin{cases} 0 & t < \tau \\ (\frac{t}{\tau})^{\beta} & t \geq \tau, \end{cases} \tag{22}$$

where $\tau \sim 10$ d is the viscosity time-scale and $\beta = -19/16$ for an electron scattering dominated disc opacity (Cannizzo, Lee & Goodman 1990). In the case of this system under the chosen parameters, the duration is about the same order of magnitude with the viscosity time-scale. Equation (22) can serve as the response of an impulse mass transfer, and the accretion rate corresponding to an arbitrary mass transfer rate as a function of time $\dot{M}_{\rm trans}(t)$ is the convolution between $\dot{M}_{\rm trans}(t)$ and equation (22):

$$\dot{M}_{\rm acc}(t) = {\rm Con}(\dot{M}_{\rm trans}, \dot{M}_{{\rm acc},\delta}). \tag{23}$$

We plot $M_{\rm trans}$ and $M_{\rm acc}$ as functions of time for different η in Fig. 4.

We expect that the accreted matter does not reach the neutron star or at least not for a long time. It is because the matter accreted on to the neutron star will quench the pulsar wind and thus destroy the emission mechanism. The accreted matter is expected to be stopped by the propeller effect of the magnetic field. The condition for the propeller effect is that the fastness parameter $f > 1$, which is defined as $f = \Omega_\star/\Omega_K(r_{\rm A})$, where $\Omega_\star$ is the angular velocity of the pulsar and $\Omega_{\rm K}(r_{\rm A})$ is the angular velocity of Kepler motion at the Alfvén radius $r_{\rm A}$. With the assumption of a typical magnetic field strength $B = 10^{12}$ G and a spin frequency $\nu > 1$, the condition of the fastness parameter is satisfied.

4 THE HE SPECTRUM AND THE LIGHT CURVE

In this section, we work on the HE spectra from AIC. With $\dot{M}_{\rm acc}$ evaluated in the above way, we calculate $t_{\rm in}$ and $r_{\rm in}$ as functions of time with equations (13) and (15). For simplicity, we assume the accretion disc is face on. Since the soft photons are mainly contributed by the inner edge of the accretion disc, we make a further simplification that the soft photons come from a ring with width of $r_{\rm in}$ at $r_{\rm in}$. Therefore,

$$n_{\rm ph}(\epsilon_0, l) = \frac{4\pi l}{h^3c^3}\frac{\epsilon_0^2 r_{\rm in}^2}{(r_{\rm in}^2 + l^2)^{3/2}(\exp\frac{\epsilon_0}{kT_{\rm in}} - 1)}. \tag{24}$$

Assuming the velocities of the electrons in the pulsar wind zone dldΩ follows a Gaussian distribution:

$$\frac{{\rm d}N(\Gamma)}{{\rm d}\Gamma {\rm d}l {\rm d}\Omega} = N_0 \exp\left(-\frac{(\Gamma - \Gamma_0)^2}{2\Delta\Gamma^2}\right), \tag{25}$$

where N_0 is normalized to the number of electrons per unit length around l:

$$\int \frac{N(\Gamma)}{{\rm d}\Gamma {\rm d}\Omega {\rm d}l}\Gamma m_{\rm e}c^2 {\rm d}\Gamma = \frac{L_{\rm pw}}{4\pi c}. \tag{26}$$

From equation (26), we have

$$N_0 = \frac{L_{\rm pw}}{4\pi c\sqrt{2\pi}}\frac{1}{\Delta\Gamma\Gamma_0 m_{\rm e}c^2}. \tag{27}$$

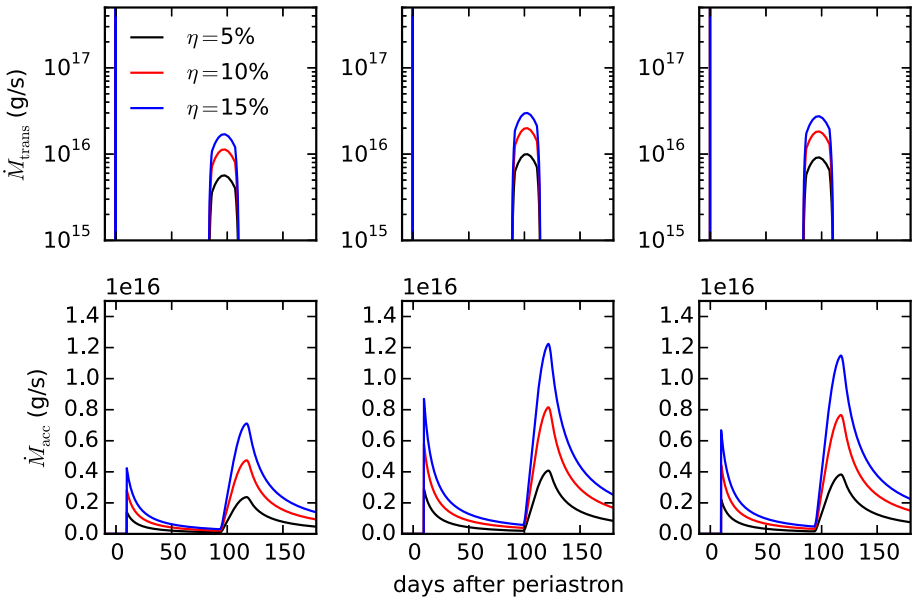

Figure 4. Upper panels: Mass transfer rate. Lower panels: The accretion rate corresponding to the mass transfer rate in the upper panel. In each panel, different η are indicated with different colours. The left, middle and right columns correspond to parameter sets 1, 2 and 3, respectively.

In principle, $\Delta\Gamma$ and Γ_0 can all be a function of l. The spectrum of AIC is

$$\frac{{\rm d}N_{\rm tot}}{{\rm d}A{\rm d}t{\rm d}\epsilon_1} = \frac{1}{D^2}\int {\rm d}l \int {\rm d}\Omega(l) \int {\rm d}\Gamma \int {\rm d}\epsilon_0 n_{\rm ph}(\epsilon_0, l)\frac{{\rm d}N(\Gamma)}{{\rm d}\Gamma {\rm d}l {\rm d}\Omega}\frac{{\rm d}N_{\Gamma,\epsilon_0}}{{\rm d}t{\rm d}\epsilon_1}, \quad (28)$$

where ${\rm d}N_{\Gamma,\epsilon_0}/{\rm d}t{\rm d}\epsilon_1$ is the kernel of AIC in the Thomson region (which is given in equation (7) of Dubus, Cerutti & Henri 2008), ϵ_0 is the energy of the soft photon and ϵ_1 is the energy of upscattered photon. $\int {\rm d}\Omega(l)$ integrates over all the incoming directions of the soft photons at wind zone l. The incoming angles of the soft photons are concentrated around

$$\cos\theta_0 \approx -\frac{l}{\sqrt{r_{\rm in}^2 + l^2}}, \quad (29)$$

and

$$\int {\rm d}\Omega \approx 2\pi \frac{l}{\sqrt{r_{\rm in}^2 + l^2}}\frac{r_{\rm in}^2}{r_{\rm in}^2 + l^2}. \quad (30)$$

Since the AIC is most efficient in a small distance range around the inner edge of the accretion disc, we assume Γ_0 and $\Delta\Gamma$ to be constant.

The evolution of the SEDs of AIC is plotted in Fig. 5 as black dashed curves with the dates labelled beside each curve. These SEDs are calculated with parameter set 2 in Table 1, $\eta = 11$ per cent, $\Gamma_0 = 2 \times 10^3$ and $\Delta\Gamma = 2 \times 10^3$. The phase-averaged SED is plotted as the red solid line. For comparison, we plot in Fig. 5 the observed SED from Li et al. (2017). The observed SED is orbital phase averaged. We plot in Fig. 6 the SEDs with different choices of Γ_0 and η.

Integrating the spectra over the HE range gives the light curve. The light curve is plotted in Fig. 7.

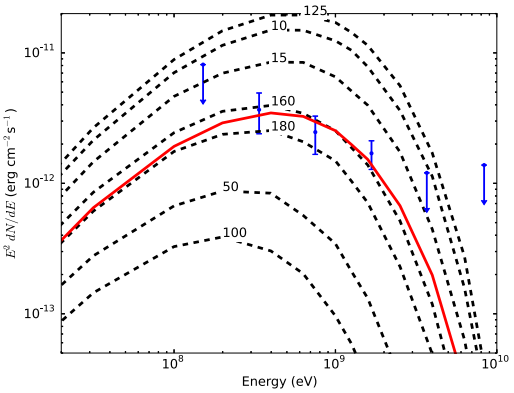

Figure 5. The evolution of the SEDs of AIC: black dashed curves are SEDs at different times. The numbers labelled beside each curve indicate the corresponding days after the periastron. The SEDs of AIC are calculated with parameter set 2 in Table 1, $\eta = 11$ per cent, $\Gamma_0 = 2 \times 10^3$ and $\Delta\Gamma = 2 \times 10^3$. The blue dots with an error bar are observed data of Li et al. (2017), and those with downward arrows are observed upper limits. The red solid curve is the phase averaged SED.

5 SUMMARY AND CONCLUSIONS

In this paper, we study the possibility that the compact companion of HESS J0632+057 is a pulsar. Under the current observational constraints, the probabilities that the compact companion has a mass less than 1.5, 2.0 and 2.4 $M_\odot$ are ~8 per cent, ~17 per cent and ~28 per cent, respectively.

In the pulsar framework, we use a new mechanism that could account for the orbital-modulated GeV emission from HESS J0632+057 (cf. Takata et al. 2017; Yi & Cheng 2017). The pulsar companion travels through the circumstellar disc of the main-sequence star twice in each orbit when some of the matter is gravity captured. The captured matter develops an accretion disc around the pulsar, and from which the soft photons are inverse Compton scattered by the pulsar wind as the GeV emission from the system.

Under assumptions of parameters within observational constraints, the above-mentioned mechanism can produce SED and light curve in accordance with current observations (see Figs 5 and 7).

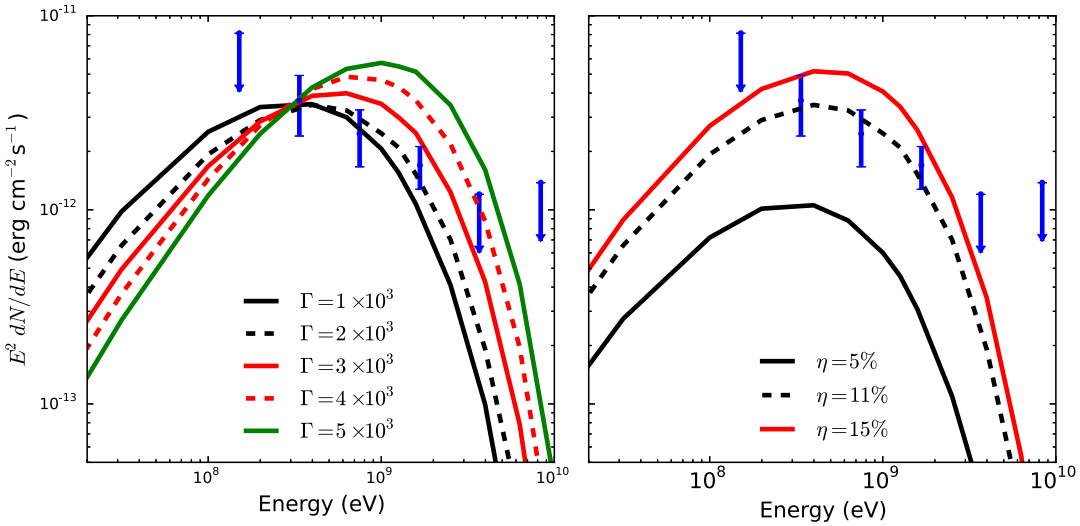

Figure 6. Same as Fig. 5, but with different Γ_0 and η. The SEDs in the left-hand panel correspond to different Γ_0 (in different line colours and styles as shown in the legend) with $\eta = 11$ per cent. The SEDs in the right-hand panel correspond to different η with $\Gamma_0 = 2 \times 10^3$.

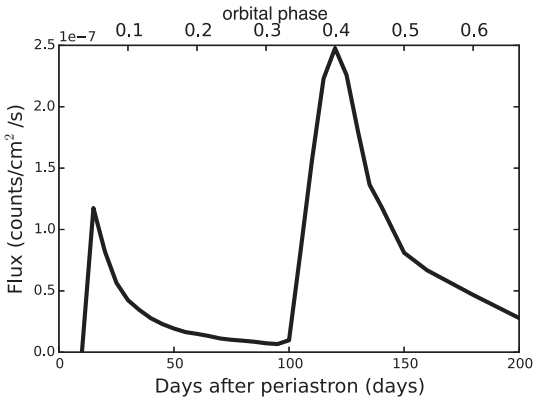

Figure 7. The light curve in the HE range. The parameters are the same as in Fig. 5.

One major prediction of the proposed mechanism is that the light curve has two peaks, the larger one is at around 0.4 after periastron, while the smaller one is between phases 0 and 0.1, with integrated flux one-fourth of the larger one.

ACKNOWLEDGEMENTS

This work is partially supported by a GRF grant under 17302315.

REFERENCES

Acciari V. A., Aliu E., Arlen T. et al., 2009, ApJ, 698, L94
Aharonian F. A., Akhperjanian A. G., Bazer-Bachi A. R. et al., 2007, A&A, 469, L1
Aleksić J., Alvarez E. A., Antonelli L. A. et al., 2012, ApJ, 754, L10
Aliu E., Archambault S., Aune T. et al., 2014, ApJ, 780, 168
Aragona C., McSwain M. V., De Becker M., 2010, ApJ, 724, 306
Bondi H., Hoyle F., 1944, MNRAS, 104, 273
Bongiorno S. D., Falcone A. D., Stroh M., Holder J., Skilton J. L., Hinton J. A., Gehrels N., Grube J., 2011, ApJ, 737, L11
Bosch-Ramon V., Khangulyan D., 2009, I. J. Mod. Phys., 18, 347
Caliandro G. A., Hill A. B., Torres D. F. et al., 2013, MNRAS, 436, 740
Cannizzo J. K., Lee H. M., Goodman J., 1990, ApJ, 351, 38
Carciofi A. C., Bjorkman J. E., 2006, ApJ, 639, 1081
Casares J., Ribó M., Ribas I., Paredes J. M., Vilardell F., Negueruela I., 2012, MNRAS, 421, 1103
Chernyakova M., Neronov A., Lutovinov A., Rodriguez J., Johnston S., 2006, MNRAS, 367, 1201
Dubus G., 2006, A&A, 456, 801
Dubus G., 2015, C. R. Phys., 16, 661
Dubus G., Cerutti B., 2013, A&A, 557, A127
Dubus G., Cerutti B., Henri G., 2008, A&A, 477, 691
Falcone A. D., Grube J., Hinton J., Holder J., Maier G., Mukherjee R., Skilton J., Stroh M., 2010, ApJ, 708, L52
Hinton J. A., Skilton J. L., Funk S. et al., 2009, ApJ, 690, L101
Kalogera V., Baym G., 1996, ApJ, 470, L61
Khangulyan D., Aharonian F. A., Bogovalov S. V., Ribó M., 2012, ApJ, 752, L17
Kong S. W., Yu Y. W., Huang Y. F., Cheng K. S., 2011, MNRAS, 416, 1067
Lee U., Osaki Y., Saio H., 1991, MNRAS, 250, 432
Li J., Torres D. F., Cheng K. S., Wilhelmi E., Kretschmar P., Hou X., Takata J., 2017, ApJ, preprint (arXiv:1707.04280)
Maraschi L., Treves A., 1981, MNRAS, 194, 1P
Moritani Y., Okazaki A. T., Carciofi A. C. et al., 2015, ApJ, 804, L32
Porter J. M., 1999, A&A, 348, 512
Rees M. J., 1988, Nature, 333, 523
Shakura N. I., Sunyaev R. A., 1973, A&A, 24, 337
Takata J., Tam P. H. T., Ng C. W., Li K. L., Kong A. K. H., Hui C. Y., Cheng K. S., 2017, ApJ, 836, 241
Waters L. B. F. M., van den Heuvel E. P. J., Taylor A. R., Habets G. M. H. J., Persi P., 1988, A&A, 198, 200
Yi S.-X., Cheng K. S., 2017, ApJ, 844, 114

This paper has been typeset from a TEX/LATEX file prepared by the author.